

Article

Film Carbon Veil-Based Electrode Modified with Triton X-100 for Nitrite Determination

Natalia Yu. Stozhko *, Maria A. Bukharinova, Ekaterina I. Khamzina, Aleksey V. Tarasov
and Sergey V. Sokolov

Department of Physics and Chemistry, Research and Innovation Center of Sensor Technologies, Ural State University of Economics, 8 Marta St., 62, Yekaterinburg 620144, Russia; m.a.bukharinova@usue.ru (M.A.B.); xei260296@mail.ru (E.I.K.); tarasov_a.v@bk.ru (A.V.T.); ssokolov@yandex.ru (S.V.S.)

* Correspondence: sny@usue.ru

Received: 15 July 2020; Accepted: 26 August 2020; Published: 28 August 2020



Abstract: A film carbon veil-based electrode (FCVE) modified with non-ionic surfactant Triton X-100 (TrX100) has been developed for nitrite determination. A new simple and producible technique of hot lamination (heat sealing) has been used for the FCVE manufacturing. The paper presents the findings of investigating the FCVE and the TrX100/FCVE by using voltammetry, chronoamperometry, and scanning electron microscopy. Modification of the electrode with TrX100 improves the hydrophilic property of its surface, which results in a larger electrode active area and higher sensitivity. Optimal conditions for nitrite determination with the use of the TrX100/FCVE have been identified. The linear range (LR) and the limit of detection (LOD) are 0.1–100 μM and 0.01 μM , respectively. The relative standard deviation (RSD) does not exceed 2.3%. High selectivity of the sensor ensures its successful application for the analysis of real samples (sausage products and natural water). The obtained results accord well with the results of the standard spectrophotometric method.

Keywords: carbon veil; hot lamination; surfactant; film sensor; nitrite; natural water; sausage products

1. Introduction

Nitrous acid salts (nitrites) are common contaminants of environmental objects (water, soil) and some food products. Sources of nitrite in the ecological environment are household wastes, animal wastes, atmospheric emissions from enterprises, as well as nitrogen-containing fertilizers used in agriculture to improve yields. Sodium nitrite/potassium nitrite (E250/E249) is one of the most commonly used food additives in food industry to preserve meat and fish products recognizable appearance. Nitrite accumulates in products of vegetable and animal origin and enters the human body with food.

Nitrite belongs to toxic substances and can cause inorganic contamination to human health. Excessive nitrite in the blood vascular system can reduce the blood capacity to transport oxygen and cause oxygen deprivation [1]. Besides, nitrite could interact with amides/amines to form harmful N-nitrosamine compounds, resulting in cancer [2,3]. This is the reason for controlling the concentration of nitrite in water and food products. Nitrite level in drinking water should not exceed 3 mg/L [4]. Sausage products may contain 50 mg of nitrite per kilogram [5].

Thus, exploiting effective means for nitrite detection in food products, biological fluids and water is essential for human health and environmental protection. Hence, different physical-chemical methods for nitrite detection have been proposed, such as chromatography [1,6], titration [7,8] spectrophotometry [9,10] and electrochemistry [11,12]. Along with obvious advantages they have some shortcomings. The chromatographic approach is labor intensive and complicated. The titration method lacks sensitivity. Spectrophotometry, though highly sensitive, requires the use of toxic and/or cancer-causing reagents [13]. Electrochemical methods have been favored over other methods of

nitrite sensing due to their high sensitivity and selectivity, simplicity, low cost, and feasibility for on-site analysis.

In electrochemical methods, the analytical signal is dependent on the state of the surface of the working electrode. It is known that the transition from a macro to a micro and nanostructured surface is accompanied by an increase in sensitivity and selectivity of measurements, and a decrease in the detection limit of the substance [14]. In order to engineer the electrode surface and improve its analytical and operational characteristics, the electrode surface is modified [15]. Various nanomaterials with special catalytic, adsorption, and energy characteristics can be applied as modifiers of electrodes intended for nitrite determination. Among them are grapheme [16,17], carbon nanotubes [15], metal [18,19] and oxide [20] nanoparticles. Sometimes in order to increase the selectivity of NO_2^- determination, macrocyclic compounds [21], enzymes [21] and combinations of different nanomaterials [22,23] can be added to sensitive layers of sensors. The disadvantages of the existing NO_2^- sensors include the use of complex and lengthy operations for processing and modifying their surface. In some cases, this process can last from 60 min [24] to 24 h [25]. Sometimes high temperature (400–700 °C) pre-treatment of the electrode is needed [26,27]. In addition, the existing nitrite sensors do not always possess good analytical characteristics; for example, the linear range of some sensors does not exceed the same order of magnitude [16,18,28].

Electroanalysis may exploit sensors of different designs and shapes. Planar sensors seem to offer potential for usage in field conditions, combined with portable equipment. Most often, they are obtained applying the screen-printed technology and using various conductive pastes and composites [29,30]. Despite relative simplicity and scalability of the screen-printed technology, its application is limited by the need to manufacture a special stencil and the use of organic solvents needed to wash it for reuse. The hot lamination technology does not have these shortcomings. It is the process of bonding two flat surfaces, one of which has a special adhesive layer to glue to the other surface. The technology of hot lamination was successfully applied by the authors to manufacture a planar sensor for ascorbic acid determination [31]. A suitable material for use in hot lamination is carbon veil, which is chemically inert, has good heat resistance, high electrical conductivity, is strongly adhesive to film polymer materials and is not costly. To date, in the academic literature we could not find any reference to carbon veil electrodes/sensors for nitrite sensing manufactured by hot lamination. Currently the existing single sensors based on carbon felt (non-woven material, similar to carbon veil, but of higher density and thickness) for nitrite detection [24,25,28,32,33] are manufactured applying a complex technology that includes labor-intensive operations of fixing felt in the electrode body and ensuring an electrical contact [24,25,33]. In addition, for sensor fabrication carbon felt has to be pretreated by repeated washing with various solvents [25], ultrasonic processing [25], and electrochemical activation [24].

The aim of this work is to develop a planar electrochemical sensor based on carbon veil with the application of the hot lamination technology for highly sensitive and rapid detection of nitrite in various objects. For that purpose a number of tasks have to be solved: (1) to manufacture the carbon veil planar electrode using hot lamination, (2) to choose a modifier to improve the analytical characteristics of the sensor, (3) to study electrochemical behavior of nitrite on the modified electrode, (4) to choose the optimal conditions for nitrite determination, (5) to test the developed sensor on real objects.

2. Materials and Methods

2.1. Reagents and Materials

All chemicals were of chemical grade purity and used as received: standard of sodium nitrite (LenReaktiv JSC, St. Petersburg, Russia), sodium nitrite (JSC Vekton, St. Petersburg, Russia), orthophosphoric acid (NevaReaktiv Ltd., St. Petersburg, Russia), acetic acid (NevaReaktiv Ltd., St. Petersburg, Russia), boric acid (Samara pharmaceutical factory, Samara, Russia), hydrochloric acid (SigmaTec, Khimki, Russia), sodium borate (AO Reachim Ltd., Moscow, Russia), potassium

ferricyanide (AO Reachim Ltd., Moscow, Russia), zinc acetate (AO Reachim Ltd., Moscow, Russia), sodium hydrate (JSC ChemReactivSnab, Ufa, Russia), sulphanilamide (Merck KGaA, Darmstadt, Germany), N-1 (1-naphthyl)-1,2-diaminoethandichloride (JSC LenReaktiv, St. Petersburg, Russia), TritonX-100 (TrX100) (Panreac Quimica SLU, Barcelona, Spain), cetyltrimethylammonium bromide (CTAB) (Sigma-Aldrich Co., St. Louis, MO, USA), sodiumdodecyl sulfate (SDS) (Sigma-Aldrich Chemie GmbH, Steinheim, Germany), citric acid (JSC ChemReactivSnab, Ufa, Russia), ascorbic acid (Sigma-Aldrich Co, St. Louis, MO, USA), glucose (NevaReaktiv Ltd., St. Petersburg, Russia), ferric chloride (III) (AO Reachim Ltd., Moscow, Russia), copper sulphate (AO Reachim Ltd., Moscow, Russia), cobalt acetate (AO Reachim Ltd., Moscow, Russia), potassium bromate (JSC LenReaktiv, St. Petersburg, Russia), Cementit universal (Merz+Benteli AG, Niederwangen, Switzerland), acetone (Ecos-1, Moscow, Russia). Deionized water with a resistivity of 18 M Ω cm was used as the solvent.

Carbon veil with surface density of 30 g/m² and surface electrical resistivity of 8–10 Ω (M-Carbo Ltd., Minsk, Belarus), as well as polyethylene terephthalate sheets (303 × 216 × 0.125 mm) (Fellows, Vietnam) were used for electrode fabrication.

2.2. Instruments

A laminator LM-260iD (Rayson Electrical MFG., Ltd., Foshan, Guangdong, China) was used for manufacturing carbon veil electrodes. Scanning electron microscopy (SEM) measurements were performed on Auriga Cross Beam microscope (Carl Zeiss NTS, Oberkochen, Germany) at 2 kV accelerating voltage. Deionized water with a resistivity of 18 M Ω cm was obtained on an Akvalab-UVOI-MF-1812 installation (JSC RPC Mediana-filter, Moscow, Russia). A magnetic stirrer with controlled heating, RCT basic (IKA-Werke, Staufen, Germany), was used to prepared aqueous extracts of sausage products. Electrochemical (voltammetric and chronoamperometric) studies were conducted on IVA-5 analyzer (IVA Ltd., Yekaterinburg, Russia). Spectrophotometric measurements were performed on ECO-VIEW UV 1200 spectrophotometer (Shanghai Mapada Instruments Co., Ltd., Shanghai, China).

2.3. Procedures

2.3.1. Phytosynthesis of Gold Nanoparticles (Phyto-Au)

An extract from strawberry leaves was used as source of antioxidants (reducers) for synthesis of gold nanoparticles [34]. To 5 mL of boiling 1 mM HAuCl₄ solution, 1 mL of freshly prepared extract from strawberry leaves was added with vigorous stirring (pH 11). Gold sol was synthesized for 5 min and then cooled to ambient temperature. The obtained nanoparticles were separated from the supernatant and resuspended in the initial volume of deionized water. The diameter of spherical phyto-Au was 14 nm [35].

2.3.2. Manufacturing of the Sensor

The sensor manufacturing procedure is shown in Figure 1. A piece of carbon veil was placed on a sheet of polyethylene terephthalate and moved between the laminator rolls heated to 140 °C. The obtained film coated with carbon veil was cut into 35 × 3 mm strips. A 293 × 206 mm section of carbon veil may result in 575 electrodes sized 35 × 3 mm. The middle part of the electrode separating the working and contact zones was covered with a mixture of cementite-acetone in a ratio of 1:5 by volume. The geometric area of the working zone of the electrode was 15 mm² (5 × 3 mm). The resulting electrode was called a film carbon veil-based electrode (FCVE).

Modification of the FCVE working zone involved the process of drop-casting of surfactant solutions (TrX100, CTAB, SDS) and phytosynthesized sol of gold nanoparticles (phyto-Au) on the electrode. When applying 10 μ L of 0.1 mM surfactant to the FCVE working area, the surfactant/FCVE was obtained. The modified phyto-Au/FCVE was obtained by applying 10 μ L phyto-Au sol to the FCVE; phyto-Au/TrX100/FCVE was obtained by applying 10 μ L of 0.1 mM TrX100 and 10 μ L phyto-Au sol. After modification, the electrodes were dried under a regular incandescent lamp.

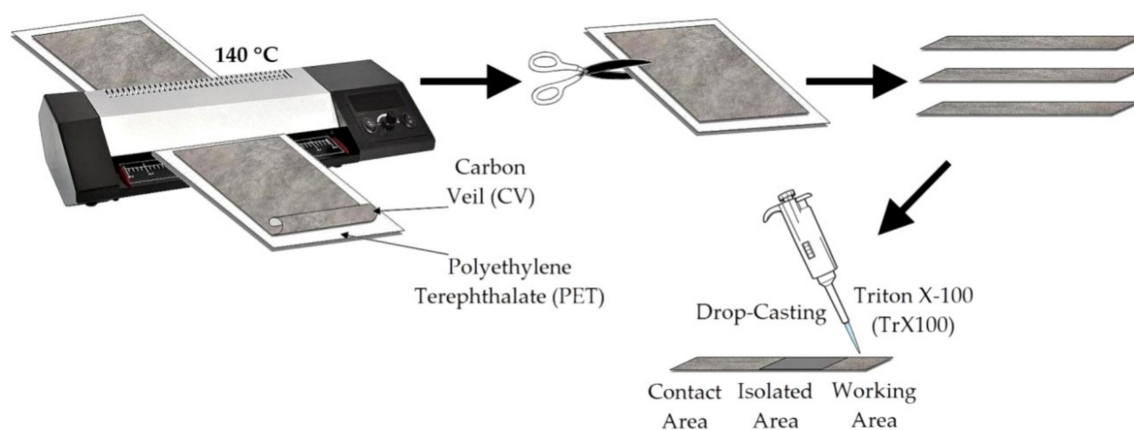


Figure 1. Manufacturing of the film carbon veil-based electrode (FCVE).

2.3.3. Electrochemical Measurements

Electrochemical studies were performed by cyclic and linear sweep voltammetry, as well as chronoamperometry in a three-electrode cell, including a silver–silver chloride reference electrode (Ag/AgCl/KCl, 3.5 M) (Gomel, Belarus), a carbon rod as an auxiliary electrode, and working electrodes FCVE and TrX100/FCVE. Working electrodes were washed with deionized water before application. Electrochemical measurements were carried out at $(24 \pm 1) ^\circ\text{C}$.

Cyclic voltammograms of NO_2^- were recorded in the potential range from 0.3 to 1.5 V on FCVE and TrX100/FCVE at a potential scan rate 0.05 Vs^{-1} .

Cyclic voltammograms $1.0 \text{ mM } [\text{Fe}(\text{CN})_6]^{3-/4-}$ were recorded in the potential range from -0.5 to $+1.2 \text{ V}$ on FCVE and TrX100/FCVE at a potential scan rate 0.05 Vs^{-1} in 0.1 M KCl .

Chronoamperometric measurements were carried out at potential $+0.9 \text{ V}$ in the solution containing $1.0 \text{ mM K}_4[\text{Fe}(\text{CN})_6] + 0.1 \text{ M KCl}$ and at a potential $+1.1 \text{ V}$ in BRB pH 3 containing 0.02 mM NO_2^- .

Linear sweep voltammograms of NO_2^- were recorded at anodic potential scanning in the range from 0.3 to 1.5 V. The potential scanning rate was varied within the range of $0.02\text{--}0.25 \text{ Vs}^{-1}$.

2.3.4. Sample Preparation

Samples of sausage products from different manufacturers were bought in the nearest supermarket. The sample preparation was carried out in accordance with the prescribed procedure [36,37]: 20 g of sausage was ground on a grater to particles of 1–2 mm in size, placed in a heat-resistant glass and filled with 40 mL of distilled water. Then, the contents of the glass were heated in a water bath at $80 ^\circ\text{C}$ for 40 min while stirring. After cooling to $20 ^\circ\text{C}$, the mixture was filtered through a blue ribbon filter. The filtrate was used for electrochemical analysis.

Samples of environmental water were tap water and water taken from wells. Water sample preparation was not performed.

2.4. Statistical Analysis and Data Treatment

All measurements were carried out three times, and the results were calculated for a confidence level of 0.95. The results are presented as $X \pm \Delta X$, where X is the average value and ΔX is the confidence interval. The recovery of NO_2^- was calculated according to IUPAC recommendations [38]. Limits of detection (LOD) and quantification (LOQ) were calculated as $3\text{SD}/b$ and $10\text{SD}/b$, respectively, where SD is the standard deviation of the response and b is the slope of the calibration graphic. F - and t -tests were used to compare the results of NO_2^- determination in water samples and sausage extracts obtained on the developed TrX100/FCVE sensor and the reference spectrophotometric method.

3. Results

3.1. Electrochemical Behavior of NO_2^- on FCVE and Modified FCVE

The electrochemical behavior of nitrite on the FCVE and modified FCVE was studied in the Britton–Robinson buffer (BRB) background electrolyte. As can be seen in Figure 2, the cyclic voltammogram registered on the FCVE (curve 1) and TrX100/FCVE (curve 3) in the BRB solution in the absence of nitrite exhibits no anodic and cathodic signals, which indicates the electrochemical inertia of the carbon veil and TrX100. The introduction of 0.02 mM NO_2^- in BRB leads to the appearance of nitrite oxidation current at 1.18 V (Figure 2, curve 2 and 4). At the same time no signals are observed on the cathodic branch of the cyclic voltammogram, which indicates irreversible oxidation of nitrite on the FCVE and TrX100/FCVE. There is a three-fold increase in the oxidation current of 0.02 mM NO_2^- on the TrX100/FCVE as compared to the FCVE (Figure 2, curve 4). The reason for this effect is that the carbon veil is a poorly wettable material, and the modification with the surfactant increases its hydrophilicity, which results in a larger active surface area of the electrode (the surface area estimate is given in Section 3.3).

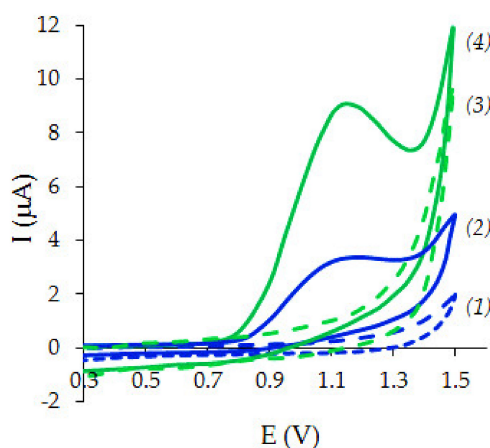


Figure 2. Cyclic voltammograms on the FCVE (1, 2) and TrX100/FCVE (3, 4), in Britton–Robinson buffer (BRB) (pH 3) in the absence (1, 3) and in the presence of 0.02 mM NO_2^- (2, 4). Potential scan rate: 0.05 Vs^{-1} .

Gold nanoparticles are widely used as electrode modifying agents that improve analytical and sensor properties of the electrode. In such a way, modification of the electrode surface with gold nanoparticles (AuNPs) can lead to better heterogeneous charge transfer ability [25]; higher conductivity [39]; larger surface area [18]; exhibition of enhanced catalytic activity [40]; and, in general, to higher sensitivity to nitrite detection. Synthesis of gold nanoparticles has a considerable impact on properties of modified electrodes. The use of gold nanoparticles synthesized with plant extracts as a reducing and stabilizing agent ensures higher sensitivity and lower limit of ascorbic acid detection in comparison with gold nanoparticles, synthesized by the Turkevich method [31]. In this respect, the study of the electrochemical behavior of nitrite on the FCVE modified with phyto-synthesized gold nanoparticles is attracting widespread interest.

Figure 3 shows cyclic voltammograms registered on the phyto-Au/FCVE and the phyto-Au/TrX100/FCVE in BRB in the presence and in the absence of NO_2^- . In the absence of nitrite in BRB, one oxidation current of gold nanoparticles is recorded at 1.26 V on the phyto-Au/FCVE and at 1.23 V on the phyto-Au/TrX100/FCVE; and one reduction current of Au(III) ions at 0.63 V and 0.50 V, respectively (Figure 3, curves 1 and 3, a dashed line). Addition of 0.02 mM NO_2^- in BRB does not result in additional signals on cyclic voltammograms (Figure 3, curves 2 and 4, a solid line), but causes a stronger and broader anodic signal registered in BRB in the absence of nitrite. It is evident that a broad anodic signal recorded in nitrite-containing solutions on the phyto-Au/FCVE and the

phyto-Au/TrX100/FCVE is the consequence of the overlap of two processes: nitrite oxidation and gold nanoparticles oxidation. The comparison of Figures 2 and 3 shows that the anodic signal recorded on the phyto-Au/FCVE and the phyto-Au/TrX100/FCVE in BRB containing NO_2^- is not of the catalytic nature. The absence of the catalytic effect in the processes of nitrite oxidation on the gold nanoparticles was reported by Brainina et al. [41]. Since modification of the FCVE and TrX100/FCVE with gold nanoparticles did not result in a strong and clear individual nitrite signal, these electrodes were not used in further work.

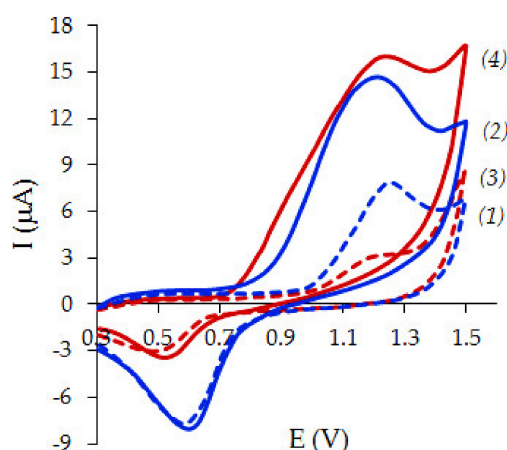


Figure 3. Cyclic voltammograms on the phytosynthesized gold nanoparticles phyto-Au/FCVE (1, 2) and phyto-Au/TrX100/FCVE (3, 4) in BRB (pH 3) in the absence (1, 3) and in the presence of 0.02 mM NO_2^- (2, 4). Potential scan rate: 0.05 Vs^{-1} .

3.2. Choice of Surfactant for FCVE Modification

Considering the positive effect of modifying the FCVE with a surfactant (Figure 2), we tested the impact of three different surfactant types—cationic (CTAB), anionic (SDS), and nonionic (TrX100)—on the nitrite electrooxidation. The range 0.01–1.0 mM of the studied concentrations correlates with the critical micellar concentrations of each surfactant at 20–25 °C which was claimed by the producer: 0.92 mM for CTAB; 7–10 mM for SDS; and 0.2–0.9 mM for TrX100. Figure 4 illustrates the dependence of the nitrite oxidation peak current (I_p) on the logarithm of surfactant concentration used for the FCVE modification.

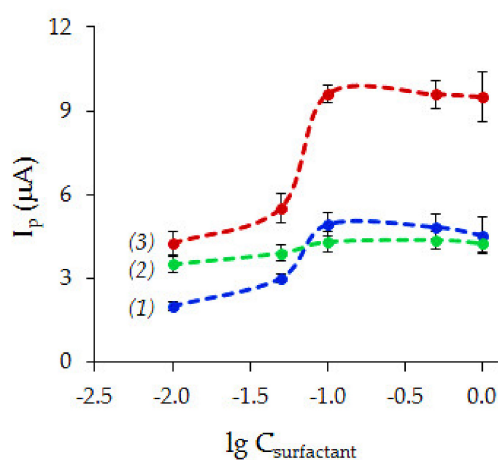


Figure 4. Dependence of the nitrite oxidation peak current on the logarithm of surfactant concentration (mM) used for the FCVE modification: cetyltrimethylammonium bromide (CTAB) (1), sodiumdodecyl sulfate (SDS) (2) and TrX100 (3). Solution: BRB (pH 3) + 0.02 mM NO_2^- .

As can be identified from Figure 4, SDS concentration on the FCVE surface does not affect the nitrite oxidation peak current. It might be due to the fact that SDS generates negative charge on the FCVE surface and repels charges of nitrite ions. The dependence $I_p = f(C_{\text{surfactant}})$ for CTAB and TrX100 can be broken into two sections. When CTAB and TrX100 concentrations grow from 0.01 to 0.1 mM, the nitrite oxidation current increases. When CTAB and TrX100 concentrations grow from 0.1 to 1.0 mM, the nitrite oxidation current stays almost the same. An increase in the nitrite oxidation current in the first section of the dependence $I_p = f(C_{\text{surfactant}})$ can be explained by a better wettability property of the FCVE caused by CTAB and TrX100 adsorption and, as a consequence, larger active electrode area. In the second section the adsorption layer of the surfactant on the FCVE surface saturates, which results in stabilization of the nitrite oxidation current. It is worth mentioning that on approaching the critical micellar concentration, the spread in nitrite oxidation current values widens by each consequent measure, which is most evident for TrX100 (Figure 4, curve 3). Since the maximum nitrite oxidation current and minimum spread in its values are observed for 0.1 mM TrX100, our choice was made in favor of the TrX100/FCVE.

3.3. Characterization of the FCVE and the TrX100/FCVE

Figure 5 presents SEM-images of the FCVE and the TrX100/FCVE surfaces. The FCVE surface (Figure 5a) looks like a fiber consisting of thin, randomly intertwined threads that are held together by a binder. The diameter of the fiber is from 5 to 10 microns. The comparison of the SEM-images shows that the SEM-images of the TrX100/FCVE (Figure 5b) do not visually differ much from the FCVE (Figure 5a).

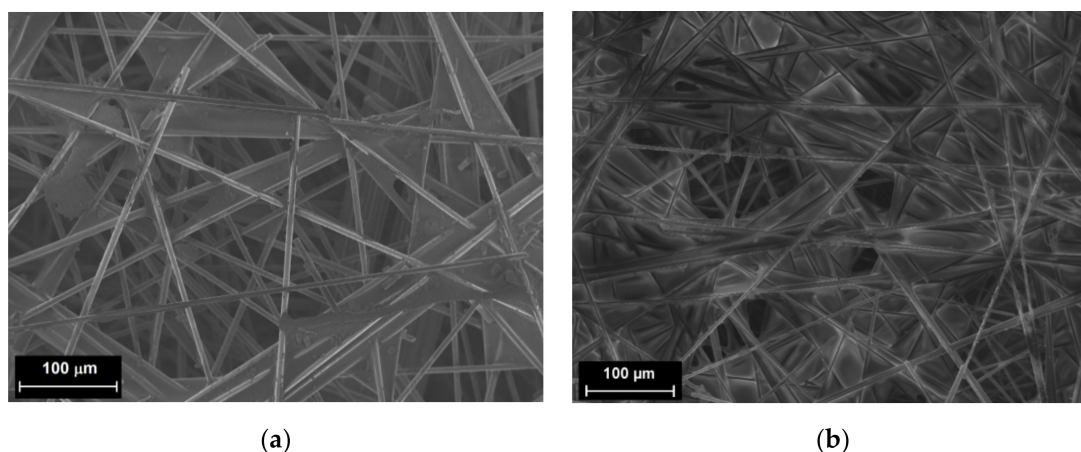


Figure 5. SEM-images of the FCVE (a) and the TrX100/FCVE (b) surfaces.

In order to select the right equation for calculating the effective surface area of the electrode, we studied electrochemical behavior of $K_4[Fe(CN)_6]$ on the TrX100/FCVE and FCVE by applying the method of cyclic voltammetry. Figure 6 illustrates cyclic voltammograms on the FCVE and the TrX100/FCVE in 0.1 M KCl containing 1 mM $K_4[Fe(CN)_6]$. Compared to the FCVE, the increase in red-ox currents of $[Fe(CN)_6]^{3-/4-}$ on the TrX100/FCVE is observed. The ratio of anodic and cathodic peak currents (I_{mpa}/I_{mpc}) is 2.35 for the FCVE and 1.34 for the TrX100/FCVE, which indicates that the rates of the anodic and cathodic processes on the TrX100/FCVE are close, in contrast to the FCVE, where the rate of the anodic process is higher than the cathodic one. The potential difference between the cathodic and anodic peaks in $[Fe(CN)_6]^{3-/4-}$ is 1.00 V and 1.13 V for the TrX100/FCVE and the FCVE, respectively, which confirms the irreversible nature of the processes. Following the results of the experiment the Cottrell equation [42] was used to measure the effective surface area of the electrodes:

$$I = nFAC \sqrt{\frac{D}{\pi t}} \quad (1)$$

where I is current (A), n is the number of electrons ($n=1$), F is Faraday's Constant ($96\,500\text{ C mol}^{-1}$), A is the electrochemical active area of the electrode (cm^2), D is the diffusion coefficient ($D = 7.6 \times 10^{-6}\text{ cm}^2\text{ s}^{-1}$) [43], C is the bulk concentration of $\text{K}_4[\text{Fe}(\text{CN})_6]$ (mol cm^{-3}) and t is time (s).

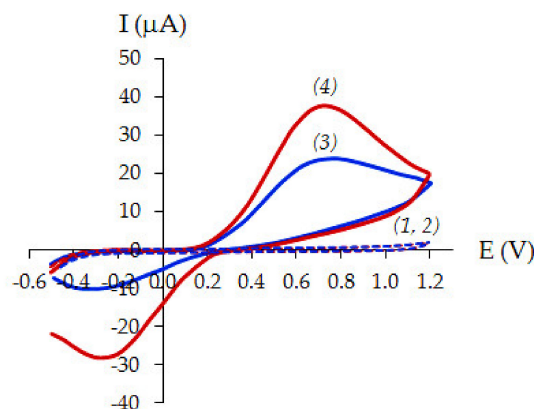


Figure 6. Cyclic voltammograms of 1 mM $\text{K}_4[\text{Fe}(\text{CN})_6]$ on (3) FCVE and (4) TrX100/FCVE and (1, 2) in a supporting 0.1 M KCl solution. Potential scan rate: 0.05 V s^{-1} .

As is given in the Cottrell Equation (1), the dependence slope $I = f(t^{-1/2})$ can be used to measure the active surface area of the electrode. To obtain the dependence $I = f(t^{-1/2})$, chronoamperograms of $\text{K}_4[\text{Fe}(\text{CN})_6]$ oxidation were recorded at the controlled potential. Then $t^{-1/2}$ was calculated for each current value on the chronoamperogram, and $I = f(t^{-1/2})$ was plotted.

Figure 7 shows chronoamperograms of $\text{K}_4[\text{Fe}(\text{CN})_6]$ oxidation at a potential of 0.9 V on the FCVE and the TrX100/FCVE (Figure 7a), as well as the dependences $I = f(t^{-1/2})$ (Figure 7b). As can be seen from Figure 7b, the slope of the linear relationship $I = f(t^{-1/2})$ for the TrX100/FCVE is 2.5 times higher than for the FCVE. According to the performed calculations, the area of the FCVE appeared to be 17 mm^2 and 40 mm^2 for the TrX100/FCVE.

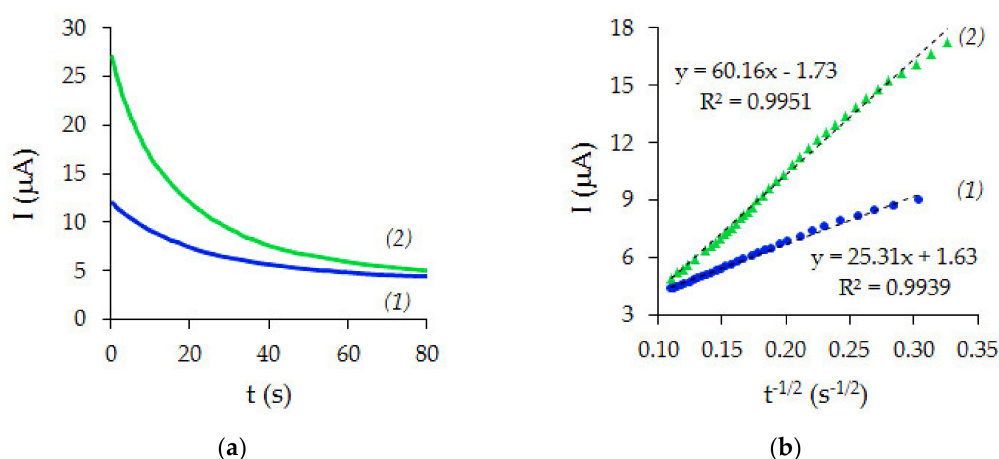


Figure 7. Chronoamperograms obtained at 0.9 V potential on the FCVE (1) and the TrX100/FCVE (2) in 0.1 M KCl containing 1.0 mM $\text{K}_4[\text{Fe}(\text{CN})_6]$ (a). Dependencies $I = f(t^{-1/2})$ are obtained from chronoamperograms on the corresponding electrodes (b).

3.4. Effect of pH

The effect of the background electrolyte pH on voltammetric characteristics of nitrite oxidation on the TrX100/FCVE was measured in the range of pH from 2 to 7. As can be seen in Figure 8, the nitrite oxidation on the TrX100/FCVE proceeds with the least overvoltage (E_p) at pH 3. In the range of pH from 3 to 7 the equation of linear regression (2) is as follows:

$$E_p \text{ (V)} = 0.0087\text{pH} + 1.1041, R^2 = 0.9084 \quad (2)$$

and shows that nitrite oxidation on the TrX100/FCVE within this pH range is almost proton-independent. Non effect of pH solution on the peak potential of nitrite oxidation was discussed by Afkhami et al. [44].

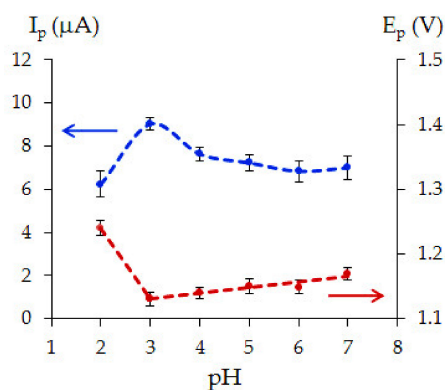
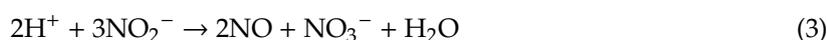


Figure 8. Effect of background electrolyte pH on the nitrite oxidation peak current (I_p) and peak potential (E_p) on the TrX100/FCVE. Solution: BRB + 0.02 mM NO_2^- .

The effect of the peak current (I_p) of nitrite oxidation on solution pH (Figure 8) accords well with the literature on the subject [25,44–46]. Oxidation current has the highest value at pH 3. A sharp decline of nitrite oxidation current at $\text{pH} < 3$ may be caused by nitrite instability in highly acidic media due to conversion of NO_2^- to NO and NO_3^- [46,47], by Equation (3):



A gradual decline of nitrite signal at $\text{pH} > 3$ might result from the formation of oxide layers on the electrode surface in basic solutions, which hinders nitrite oxidation [44]. Taking into consideration the evidence supporting participation of one electron in the nitrite oxidation process in acidic media [25], the electrode reaction is proposed as follows Equation (4):



As can be seen from this reaction, the nitrite ion loses one electron and generates nitrogen dioxide molecules that can accumulate on the electrode surface in due course. Brainina et al. [41] reported that nitrite ion electrooxidation on macro- and nanostructured electrode surfaces is not of catalytic nature, but is complicated by passivation of the electrode with an adsorbed product of an electrochemical reaction. The further studies were performed using BRB with pH 3.

3.5. Effect of Potential Scan Rate

The effect of the potential scan rate in the range from 20 to 250 mVs^{-1} on the peak current and the peak potential of nitrite electrooxidation are given in Figure 9. As the scan rate grows, the peak current of nitrite oxidation increases and the peak potential shifts to the anodic region (Figure 9), which indicates the irreversible electrode process [43]. Dependence of the peak potential on the natural logarithm of the potential scan rate is expressed by Equation (5):

$$E_p \text{ (V)} = (1.57 \pm 0.07) + (0.13 \pm 0.01) \ln v, R^2 = 0.9756. \quad (5)$$

The process of nitrite electrooxidation on the TrX100/FCVE is diffusion-controlled, which is confirmed by the linear dependence of the nitrite oxidation peak current on the square root of the scan rate, which is expressed by Equation (6):

$$I_p (\mu\text{A}) = (45.58 \pm 0.95)v^{1/2} (\text{Vs}^{-1}) - (0.85 \pm 0.04), R^2 = 0.9979. \quad (6)$$

This conclusion also confirms the dependence of the natural logarithm of the nitrite oxidation peak current on the natural logarithm of the potential scan rate, expressed by Equation (7):

$$\ln I_p = (3.81 \pm 0.11) + (0.52 \pm 0.02)\ln v, R^2 = 0.9969. \quad (7)$$

The slope of the dependence $\ln I_p = f(\ln v)$ is 0.52 and is close to the theoretical value of 0.5, which is characteristic of a diffusion-controlled process [48].

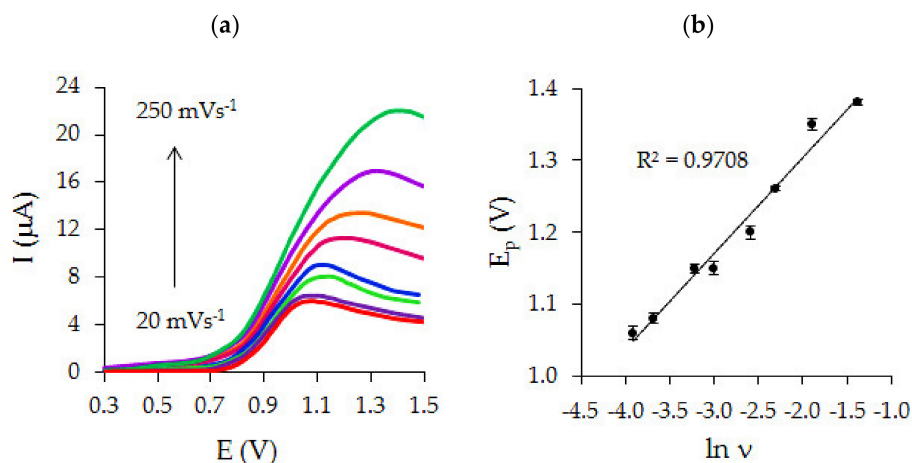


Figure 9. Linear sweep voltammograms of the TrX100/FCVE in BRB (pH 3) containing 0.02 mM NO_2^- at different potential scan rates (0.02, 0.025, 0.04, 0.05, 0.075, 0.1, 0.15, 0.25 Vs^{-1}) (a) and dependence of the oxidation peak potential on the natural logarithm of the potential scan rate (b).

The nitrite diffusion coefficients for the FCVE and TrX100/FCVE were calculated using the Cottrell Equation (1) based on a chronoamperogram recorded at $E = 1.1$ V in BRB (pH 3) containing 0.02 mM NO_2^- and the corresponding dependence $I = f(t^{-1/2})$ (Figure 10). The value of the nitrite diffusion coefficient for the TrX100/FCVE was found as $2.24 \times 10^{-5} \text{ cm}^2 \text{ s}^{-1}$, which accords with the same order of magnitude given at modified carbon paste electrode in other studies [11,49]. For the FCVE the value of D was found $1.52 \times 10^{-7} \text{ cm}^2 \text{ s}^{-1}$.

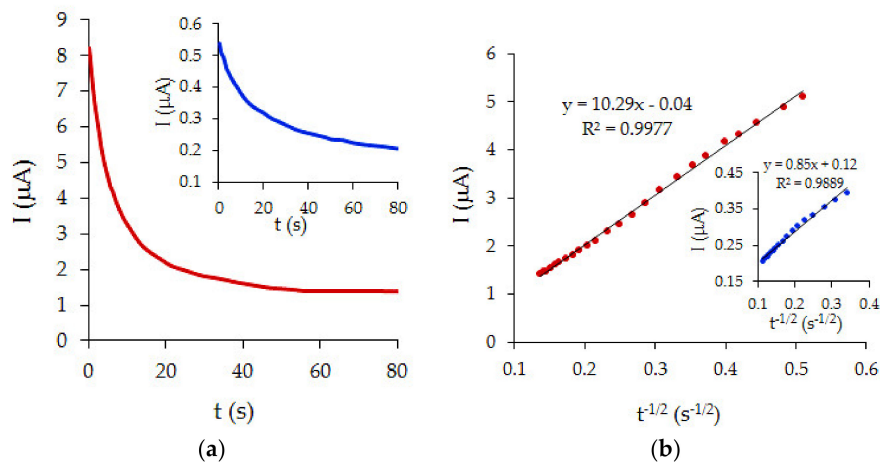


Figure 10. Chronoamperograms obtained at potential 1.1 V on the TrX100/FCVE in BRB (pH 3) containing 0.02 mM NO_2^- (a) and corresponding dependence $I = f(t^{-1/2})$ (b). Inset: (a) chronoamperograms obtained at potential 1.1 V on the FCVE in BRB (pH 3) containing 0.02 mM NO_2^- and (b) corresponding dependence $I = f(t^{-1/2})$.

3.6. Analytic Characteristics of TrX100/FCVE

Figure 11 shows voltammograms of nitrite oxidation on the TrX100/FCVE at different concentrations of NO_2^- in BRB and the corresponding dependence of the peak current on nitrite concentration. It was found that the dependence $I_p = f(C_{\text{NO}_2^-})$ is linear in the range from 0.1 to 0.9 μM and from 0.9 to 100 μM and is expressed by Equations (8) and (9), respectively:

$$I_p = (3.46 \pm 0.15)C_{\text{NO}_2^-} - (0.13 \pm 0.01), R^2 = 0.9963 \quad (8)$$

$$I_p = (0.26 \pm 0.01)C_{\text{NO}_2^-} + (2.96 \pm 0.09), R^2 = 0.9957 \quad (9)$$

The existence of two slopes of the dependence $I_p = f(C_{\text{NO}_2^-})$ may be linked with NO_2^- adsorption on the electrode surface with increase in concentration, which makes the diffusion of the analyte more difficult, as reported previously in the literature [16,20,50].

The determined sensitivity for these ranges of NO_2^- concentrations was 3.46 and 0.26 $\mu\text{A}\mu\text{M}^{-1}$, respectively. LOD and LOQ were 0.01 and 0.03 μM , respectively. The relative standard deviation (RSD) of 0.2 mM NO_2^- response is 1.1%. The proposed sensor provides stability of the analytical signal for a month, over this period it decreases by 6–9%.

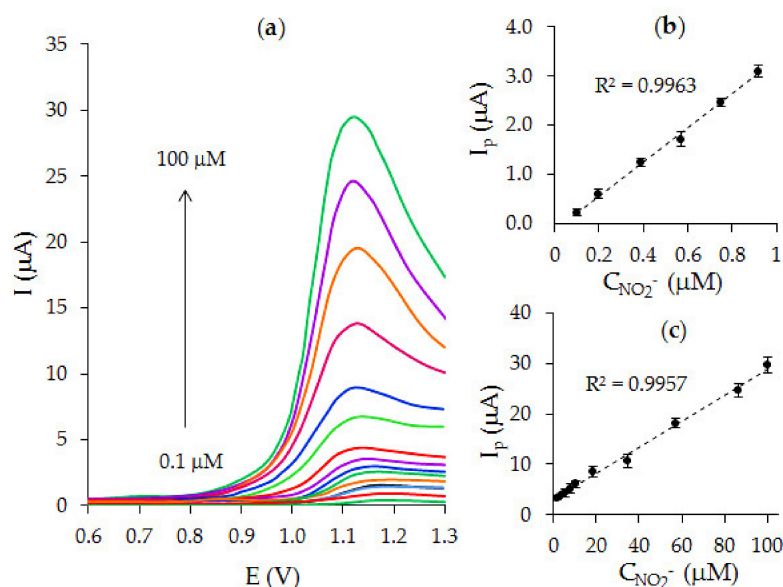


Figure 11. Linear sweep voltammograms of the TrX100/FCVE at different nitrite concentrations (a) and corresponding dependences I_p vs. $C_{\text{NO}_2^-}$ on the TrX100/FCVE (b,c).

While measuring the TrX100/FCVE selectivity, we studied the impact of those various foreign species that could be present in real samples of sausage products and water, on the response from 5 μM of nitrites. Herewith, the concentration of foreign species that could change the nitrite response by $\pm 5\%$, was considered non-interfering. The results of checking selectivity of the electrode toward nitrites are presented in Table 1. It can be seen that a 200-fold excess of glucose, Fe(III) ions, chloride and sulfate anions; a 100-fold excess of acetate ions; a 85-fold excess of Co(II); a 30-fold excess of Ni(II) and Cu(II); a 22-fold excess of BrO_3^- ; and a 10-fold excess of ascorbic and citric acids do not interfere with nitrite response. Thus, the developed sensor can tolerate a high concentration of interfering ions and, therefore, can be applied in the analysis of real samples.

Table 1. Interfering effect of various foreign species on nitrite response (nitrite response at $C_{NO_2^-} = 5 \mu M$ taken as 100%).

Interfering Substance	Concentration of Interfering Substance, μM	Response Change, %
Glucose	1000	0.0
Cl ⁻	1000	0.0
SO ₄ ²⁻	1000	0.0
Fe(III)	1000	0.0
CH ₃ COO ⁻	500	0.0
Co(II)	425	-3.1
Ni(II)	150	-4.5
Cu(II)	150	-3.3
BrO ₃ ⁻	110	-2.3
Citric acid	50	-2.9
Ascorbic acid	50	-0.5

Table 2 compares the analytical characteristics of the proposed carbon veil-based electrode and existing screen-printed sensors.

Table 2. Analytical characteristics of nitrite determination in real samples for different sensors.

Sensor *	Limit of Detection, μM	Linear Range, μM	Technique **	Sample	Ref.
GO/PEDOT:PSS/SPCE	0.018	0.05–16.55	Am	background solution	[16]
rGO/AuNPs/SPCE	0.13	1–6000	DPV, CV	purified water, packaged mineral water, dried shrimps, cured/salted fish, sausage	[17]
AuNPs-PEI/GSPE	1.0	1–10	DPV	background solution	[18]
CuAgNPs/SPCE _{anodized}	11.1/15.6	20–370	CV	tap water, river water, deionized water	[19]
MnO ₂ /GO-SPCE	0.09	0.1–1 1–1000	Am	tap water, packaged water	[20]
GR+ β -CD/SPCE	0.26	0.7–2150	Am	drinking water, tap water	[21]
AgMCs-PAA/PVA/SPCE	4.45	2–800	FI-Am	ham, bacon, fermented pork, and sausage	[22]
Ag/rGO/ β -CD/SPCE	0.24	1–2000	LSV	spiked pickles	[23]
EACFE	1.0	1.0–1000	Cm	background solution	[24]
AuNPs/GCFE	0.95	1.0–3350	CV	mustard	[25]
ACFPE	0.07	0.1–3838.5	Am	mineral water, sausage	[26]
PB/[Bmim][BF ₄]-GFE	0.013	1.0–8.0	CV	tap water	[28]
CFE	0.03	0.25–3838.5	Am	mineral water, sausage	[32]
SmFeO ₃ /CFE	50	50–1000	Am	background solution	[33]
rGO/ β -CD/CdS/SPCE	0.021	0.05–447	Am	tap water and river water	[51]
MWCNT/SPE	0.02	1–500	DPV, Am	saliva, urine, and blood samples	[52]
AuNPs/PMB/PGE	0.314	5–5000	DPV	sausage, mineral water	[53]
ccNiR + carbon ink/SPE	1.2	0.7–370	CV	drinking water, tap water, milk, urine, plasma	[54]
TrX100/FCVE	0.01	0.1–0.9 0.9–100	LSV	sausage products, water	this paper

* GO—graphene oxide; PEDOT:PSS—poly(3,4 ethylenedioxythiophene): polystyrene sulfonat; SPCE—screen-printed carbon electrode; rGO—reduced graphene oxide; β -CD— β -cyclodextrin; AuNPs—gold nanoparticles; MWCNT—multi-walled carbon nanotube; SPE—screen-printed electrode; PEI—polyethyleneimine; SPE—graphite screen printed electrodes; CuAgNPs—copper-silver nanoparticles; PMB—poly(methylene blue); PGE—pencil graphite electrode; GR—graphite; ccNiR—cytochrome c nitrite reductase; AgMCs—silver microcubics; PAA/PVA—polyacrylic acid/poly vinyl alcohol; ACFPE—annealed carbon fiber paper electrode; CFE—carbon felt electrode; EACFE—electrochemical activated carbon felt electrode; PB—Prussian blue; [Bmim][BF₄]-1-butyl-3-methylimidazolium tetrafluoroborate; GCFE—graphitizing carbon felt electrode. ** Am—amperometry; Cm—coulometry; CV—cyclic voltammetry; DPV—differential pulse voltammetry; FI-Am—flow injection amperometry; LSV—linear sweep voltammetry.

It can be seen from Table 2 that the detection limit, which is an important characteristic of the developed sensor, is not only comparable, but is even better than that of other modified electrodes. The other distinctive feature of the proposed carbon veil sensor is its inexpensiveness, as it is made

of cheap materials and with simple production technology (575 electrodes for 10 min). All these features allow the use of this sensor as disposable.

3.7. Determination of Nitrite in Real Samples

3.7.1. Analysis of Sausage Products

The electrodes were immersed into an electrochemical cell containing 9.0–9.5 mL of BRB (pH = 3), and a background voltammogram was recorded. An aliquot of the sausage extract (0.5–1.0 mL), obtained as described in Section 2.3.4, was added, thoroughly mixed, and a linear voltammogram was recorded from 0.3 to 1.5 V at a scan rate of 0.05 Vs⁻¹. The measurements were taken three times. Then additives of a standard nitrite solution were added to the cell and the corresponding voltammograms were registered. The content of NO₂⁻ was found by applying the additional method. The impact of the matrix on nitrite determination was evaluated by the added-found method.

Table 3 presents the results of the NO₂⁻ concentration analysis of the sausage extracts on the proposed sensor. High recovery (93–95%) demonstrates that the proposed sensor could be well applied for NO₂⁻ sensing in sausage extracts.

Table 3. Results of nitrite determination in sausage extracts by applying the TrX100/FCVE ($n = 3$, $p = 0.95$) and the added-found method.

Sample	Found in Extract, μM	Added, μM	Found in Extract with Additive, μM	Found Additive, μM	R, %
Sausages	24 \pm 2	20	43 \pm 1	19 \pm 1	93
“Doctorskaya” sausage	88 \pm 1	80	163 \pm 1	76 \pm 5	95
“Molochnaya” sausage	228 \pm 6	300	512 \pm 19	284 \pm 17	95

Validation of the techniques for nitrite determination in sausage extracts with the TrX100/FCVE was performed by comparing the obtained results with the findings of the standard UV-spectroscopic method [55]. The latter is based on red-coloring of a solution containing nitrite by adding 4-aminobenzenesulfamide and N-1(1-naphthyl)-1,2-diaminoethandihydrochloride and the consequent photometric measurement at a wavelength of 538 nm. This comparison is illustrated in Table 4. The RSD values confirm high precision of the data obtained. *F*- and *t*-tests data are less than critical values at $p = 0.95$ confirming the absence of systematic errors in determinations.

Table 4. Results of NO₂⁻ determination in sausage extracts applying the TrX100/FCVE and the UV-spectroscopic method ($n = 3$, $p = 0.95$).

Sample	Voltammetry with TrX100/FCVE, μM	RSD, %	Spectrophotometry, μM	RSD, %	<i>F</i> -Test	<i>t</i> -Test
Sausages	24 \pm 2	2.6	23 \pm 1	1.5	3.21	2.29
“Doctorskaya” sausage	88 \pm 1	0.5	87 \pm 2	0.8	3.45	0.08
“Molochnaya” sausage	228 \pm 6	1.2	239 \pm 11	1.9	3.02	2.43

$$F_{\text{crit}} = 19.00 (P = 0.95; df_1 = 2, df_2 = 2), t_{\text{crit}} = 2.78, P = 0.95; df = 4.$$

3.7.2. Analysis of Water Samples

The determination of initial nitrite concentrations in water was performed in the same way as described in Section 3.7.1. A water sample (2.5 mL) was added with nitrite as nitrite-ions were not detected in natural water.

The applicability of the developed TrX100/FCVE was tested on the spiked natural water (Table 5). The accuracy of nitrite sensing was tested using the added-found method. The relative standard deviation in the range of 1.1–2.3 and recovery of 98–103% confirm the absence of the random errors and high accuracy of nitrite determination.

Table 5. Determination of NO_2^- in water samples, using the TrX100/FCVE ($n = 3, p = 0.95$).

Water Sample	Added, μM	Found, μM	RSD, %	R, %
Sample 1	0.99	1.02 ± 0.06	2.3	103
Sample 2	4.95	4.87 ± 0.31	1.9	98
Sample 3	10.0	9.8 ± 0.2	1.1	99

Validation of the techniques for nitrite determination in water samples with the TrX100/FCVE was performed by comparing the obtained results with the findings of the standard UV-spectroscopic method [56]. The latter is based on the interaction of nitrite with 4-aminobenzenesulfamide in the presence of ortho-phosphoric acid (pH 1.9) and the consequent formation of a colored compound detected at a wavelength of 540 nm. This comparison is illustrated in Table 6. As can be observed in Table 6, the RSD value for the TrX100/FCVE does not exceed 2.3%. The values obtained by both techniques concur quite well. *F*- and *t*-tests data are less than critical values at $P = 0.95$ confirming the absence of systematic errors in determinations.

Table 6. Results of NO_2^- determination in water samples applying the TrX100/FCVE and the UV-spectroscopic method ($n = 3, p = 0.95$).

Water Sample	Voltammetry with TrX100/FCVE, μM	RSD, %	Spectrophotometry, μM	RSD, %	<i>F</i> -Test	<i>t</i> -Test
Sample 1	1.02 ± 0.06	2.3	0.96 ± 0.12	4.9	4.19	1.32
Sample 2	4.87 ± 0.31	1.9	5.15 ± 0.34	2.7	2.18	1.90
Sample 3	9.8 ± 0.2	1.1	9.3 ± 0.5	2.2	4.33	2.67

$$F_{\text{crit}} = 19.00 (P = 0.95; df_1 = 2; df_2 = 2), t_{\text{crit}} = 2.78; P = 0.95; df = 4.$$

4. Conclusions

A new sensor based on a carbon veil, modified with TrX100, for determination of nitrite is described. A simple and producible technique of hot lamination (heat sealing) ensures fast and mass production of disposable carbon veil electrodes at low cost. Miniature size of the sensor makes it highly promising for application in portable equipment for field conditions. The developed sensor is characterized by a wide linear range, a low detection limit, and a good reproducibility of measurements. High selectivity of the sensor ensures its successful application for the analysis of sausage products and natural water.

Author Contributions: Discussion and interpretation of the results, preparation of the final text N.Y.S.; carrying out experimental work and discussion of the results E.I.K.; writing—original manuscript M.A.B.; editing of the text A.V.T.; manufacturing sensor's transducer S.V.S. All authors have read and agreed to the published version of the manuscript.

Funding: This research received no external funding.

Conflicts of Interest: The authors declare no conflict of interest.

References

1. Genualdi, S.; Matos, M.; Mangrum, J.; de Jager, L.S. Investigation into the concentration and sources of nitrates and nitrites in milk and plant-based powders. *J. Agric. Food Chem.* **2020**, *68*, 1725–1730. [[CrossRef](#)]
2. Song, P.; Wu, L.; Guan, W. Dietary nitrates, nitrites, and nitrosamines intake and the risk of 400 gastric cancer: A meta-analysis. *Nutrients* **2015**, *7*, 9872–9895. [[CrossRef](#)]
3. Barry, K.H.; Jones, R.R.; Cantor, K.P. Ingested nitrate and nitrite and bladder cancer in northern new England. *Epidemiology* **2020**, *31*, 136–144. [[CrossRef](#)]
4. WHO. Nitrate and nitrite in drinking-water. In *Background Document for Preparation of WHO Guidelines for Drinking-Water Quality*; World Health Organization: Geneva, Switzerland, 2011.
5. State Standard 33673-2015. Cooked sausages. In *General Specifications*; Izdatelstvo Standartinform: Moscow, Russian, 2016.

6. Murray, E.; Roche, P.; Briet, M.; Moore, B.; Morrin, A.; Diamond, D.; Paull, B. Fully automated, low-cost ion chromatography system for in-situ analysis of nitrite and nitrate in natural waters. *Talanta* **2020**, *216*, 120955. [[CrossRef](#)]
7. Lenghartova, K.; Lauko, L.; Cacho, F.; Beinrohr, E. Determination of nitrites in water by in-electrode coulometric titration in reticulated vitreous carbon electrode. *Acta Chim. Slov.* **2015**, *62*, 152–158. [[CrossRef](#)]
8. He, Z.K.; Fuhrmann, B.; Spohn, U. Precise and sensitive determination of nitrite by coulometric back titration under flow conditions. *Fresenius J. Anal. Chem.* **2000**, *367*, 264–269. [[CrossRef](#)]
9. Li, Y.-S.; Zhao, C.-L.; Li, B.-L.; Gao, X.-F. Evaluating nitrite content changes in some Chinese home cooking a newly-developed CDs diazotization spectrophotometry. *Food Chem.* **2020**, *330*, 127151. [[CrossRef](#)]
10. Abou-Melha, K.S. Analytical chemistry optical chemosensor for spectrophotometric determination of nitrite in wastewater. *Chem. Select.* **2020**, *5*, 6216–6223. [[CrossRef](#)]
11. Nithyayini, K.N.; Harish, M.N.K.; Nagashree, K.L. Electrochemical detection of nitrite at NiFe₂O₄ nanoparticles synthesized by solvent deficient method. *Electrochim. Acta* **2019**, *317*, 701–710. [[CrossRef](#)]
12. Peng, Z.W.; Yuan, D.; Jiang, Z.W.; Li, Y.F. Novel metal-organic gels of bis(benzimidazole)-based ligands with copper(II) for electrochemical selectively sensing of nitrite. *Electrochim. Acta* **2017**, *238*, 1–8. [[CrossRef](#)]
13. Yenil, N.; Yemiş, F. Nitrite in nature: Determination with polymeric materials. *Pak. J. Anal. Environ. Chem.* **2018**, *19*, 104–114. [[CrossRef](#)]
14. Stozhko, N.Y.; Malakhova, N.A.; Byzov, I.V.; Brainina, K.Z. Electrodes in stripping voltammetry: From a macro- to a micro- and nano-structured surface. *J. Anal. Chem.* **2009**, *64*, 1148–1157. [[CrossRef](#)]
15. Brainina, K.; Stozhko, N.; Bukharinova, M.; Vikulova, E. Nanomaterials: Electrochemical properties and application in sensors. *Phys. Sci. Rev.* **2019**, *3*, 8050.
16. Su, C.-H.; Sun, C.-L.; Liao, Y.-C. Printed combinatorial sensors for simultaneous detection of ascorbic acid, uric acid, dopamine, and nitrite. *ACS Omega* **2017**, *2*, 4245–4252. [[CrossRef](#)]
17. Jian, J.-M.; Fu, L.; Ji, J.; Lin, L.; Guo, X.; Ren, T.-L. Electrochemically reduced graphene oxide/gold nanoparticles composite modified screen-printed carbon electrode for effective electrocatalytic analysis of nitrite in foods. *Sens. Actuators B* **2018**, *262*, 125–136. [[CrossRef](#)]
18. Talbi, M.; Al-Hamry, A.; Teixeira, P.R.; Bouhamed, A.; Azzouzi, S.; Paterno, L.G.; Kanoun, O. Graphite screen printed electrodes functionalized with AuNPs-PEI for nitrite detection. In Proceedings of the 16th International Multi-Conference on Systems, Signals & Devices (SSD), Istanbul, Turkey, 21–24 March 2019; pp. 607–610.
19. Lo, N.-C.; Sun, I.-W.; Chen, P.-Y. CuAg nanoparticles formed in situ on electrochemically pre-anodized screen-printed carbon electrodes for the detection of nitrate and nitrite anions. *J. Chin. Chem. Soc.* **2018**, *65*, 928–988. [[CrossRef](#)]
20. Jaiswal, N.; Tiwari, I.; Foster, C.W.; Banks, C.E. Highly sensitive amperometric sensing of nitrite utilizing bulk-modified MnO₂ decorated graphene oxide nanocomposite screen-printed electrodes. *Electrochim. Acta* **2017**, *227*, 255–266. [[CrossRef](#)]
21. Palanisamy, S.; Thirumalraj, B.; Chen, S.-M. A novel amperometric nitrite sensor based on screen printed carbon electrode modified with graphite/ β -cyclodextrin composite. *J. Electroanal. Chem.* **2016**, *760*, 97–104. [[CrossRef](#)]
22. Promsuwan, K.; Thavarungkul, P.; Kanatharana, P.; Limbut, W. Flow injection amperometric nitrite sensor based on silver microcubics-poly (acrylic acid)/poly (vinyl alcohol) modified screen printed carbon electrode. *Electrochim. Acta* **2017**, *232*, 357–369. [[CrossRef](#)]
23. Zhe, T.; Sun, X.; Wang, Q.; Liu, Y.; Li, R.; Li, F.; Wang, L. A screen printed carbon electrode modified with a lamellar nanocomposite containing dendritic silver nanostructures, reduced graphene oxide, and β -cyclodextrin for voltammetric sensing of nitrite. *Microchim. Acta* **2019**, *186*, 319. [[CrossRef](#)]
24. Kuntolaksone, S.; Matsuura, H. Coulometric analysis of nitrite using electrochemically activated carbon felt electrode. *Sens. Mater.* **2019**, *31*, 1215–1224. [[CrossRef](#)]
25. Wei, W.; Wu, S.-G. Study of electrooxidation behavior of nitrite on gold nanoparticles/graphitizing carbon felt electrode and its analytical application. *Chin. J. Anal. Chem.* **2019**, *47*, e19014–e19020. [[CrossRef](#)]
26. Zhu, W.; Zhang, Y.; Gong, J.; Ma, Y.; Sun, J.; Li, T.; Wang, J. Surface engineering of carbon fiber paper toward exceptionally high-performance and stable electrochemical nitrite sensing. *ACS Sens.* **2019**, *4*, 2980–2987. [[CrossRef](#)] [[PubMed](#)]

27. Muthumariappan, A.; Govindasamy, M.; Chen, S.-M.; Sakthivel, K.; Mani, V. Screen-printed electrode modified with a composite prepared from graphene oxide nanosheets and Mn_3O_4 microcubes for ultrasensitive determination of nitrite. *Microchim. Acta* **2017**, *184*, 3625–3634. [[CrossRef](#)]
28. Wang, L.; Tricard, S.; Cao, L.; Liang, Y.; Zhao, J.; Fang, J.; Shen, W. Prussian blue/1-butyl-3-methylimidazolium tetrafluoroborate–graphite felt electrodes for efficient electrocatalytic determination of nitrite. *Sens. Actuators B* **2015**, *214*, 70–75. [[CrossRef](#)]
29. Kunpatee, K.; Traipop, S.; Chailapakul, O.; Chuanuwatanakul, S. Simultaneous determination of ascorbic acid, dopamine and uric acid using grapheme quantum dots/ionic liquid modified screen-printed carbon electrode. *Sens. Actuators B* **2020**, *314*, 128059. [[CrossRef](#)]
30. Pérez-Fernández, B.; Costa-García, A.; De La Escosura-Muñiz, A. Electrochemical (bio)sensors for pesticides detection using screen-printed electrodes. *Biosensors* **2020**, *10*, 32.
31. Brainina, K.; Bukharinova, M.A.; Stozhko, N.Y.; Sokolkov, S.V.; Tarasov, A.V.; Vidrevich, M.B. Electrochemical sensor based on a carbon veil modified by phytosynthesized gold nanoparticles for determination of ascorbic acid. *Sensors* **2020**, *20*, 1800. [[CrossRef](#)]
32. Zhang, Y.; Zhu, W.; Wang, Y.; Ma, Y.; Sun, J.; Li, T.; Ji, Y. High-performance electrochemical nitrite sensing enabled by the commercial carbon fiber cloth. *Inorg. Chem. Front.* **2019**, *6*, 1501–1506. [[CrossRef](#)]
33. Yatsunami, T.; Takase, S.; Shimizu, Y. Amperometric nitrite-ion sensor based on electrodeposited Sm-based perovskite-type oxide thick-film electrode. *Sens. Mater.* **2016**, *28*, 777–784.
34. Brainina, K.; Stozhko, N.; Bukharinova, M.; Khamzina, E.; Vidrevich, M. Potentiometric method of plant microsuspensions antioxidant activity determination. *Food. Chem.* **2019**, *278*, 653–658. [[CrossRef](#)] [[PubMed](#)]
35. Stozhko, N.Y.; Bukharinova, M.A.; Khamzina, E.I.; Tarasov, A.V.; Vidrevich, M.B.; Brainina, K.Z. The effect of the antioxidant activity of plant extracts on the properties of gold nanoparticles. *Nanomaterials* **2019**, *9*, 1655. [[CrossRef](#)] [[PubMed](#)]
36. Balasubramanian, P.; Settu, R.; Chen, S.-M.; Chen, T.-W.; Sharmila, G. A new electrochemical sensor for highly sensitive and selective detection of nitrite in food samples based on sonochemical synthesized Calcium Ferrite ($CaFe_2O_4$) clusters modified screen printed carbon electrode. *J. Colloid Interface Sci.* **2018**, *524*, 417–426. [[CrossRef](#)] [[PubMed](#)]
37. Yildiz, G.; Oztekin, N.; Orbay, A.; Senkal, F. Voltammetric determination of nitrite in meat products using polyvinylimidazole modified carbone paste electrode. *Food Chem.* **2014**, *152*, 245–250. [[CrossRef](#)] [[PubMed](#)]
38. Burns, D.T.; Danzer, K.; Townshend, A. Use of the terms “recovery” and “apparent recovery” in analytical procedures (IUPAC Recommendations 2002). *Pure Appl. Chem.* **2003**, *74*, 2201–2205. [[CrossRef](#)]
39. Chen, H.; Yang, T.; Liu, F.; Li, W. Electrodeposition of gold nanoparticles on Cu-based metal-organic framework for the electrochemical detection of nitrite. *Sens. Actuators B* **2018**, *286*, 401–407. [[CrossRef](#)]
40. Pan, F.; Chen, D.; Zhuang, X.; Wu, X.; Luan, F.; Zhang, S.; Li, X. Fabrication of gold nanoparticles/l-cysteine functionalized graphene oxide nanocomposites and application for nitrite detection. *J. Alloys Compd.* **2018**, *744*, 51–56. [[CrossRef](#)]
41. Brainina, K.Z.; Galperin, L.G.; Bukharinova, M.A.; Stozhko, N.Y. Mathematical modeling and experimental study of electrode processes. *J. Solid State Electrochem.* **2014**, *19*, 599–606. [[CrossRef](#)]
42. Fotouhi, L.; Fatollahzadeh, M.; Heravi, M.M. Electrochemical behavior and voltammetric determination of sulfaguandine at a glassy carbon electrode modified with a multi-walled carbon nanotube. *Int. J. Electrochem. Sci.* **2012**, *7*, 3919–3928.
43. Bard, A.J.; Faulkner, L.R. *Electrochemical Methods: Fundamentals and Applications*, 2nd ed.; John Wiley & Sons Inc: Hoboken, NJ, USA, 2001.
44. Afkhami, A.; Soltani-Felehgari, F.; Madrakian, T.; Ghaedi, H. Surface decoration of multi-walled carbone nanotubes modified carbone paste electrode with gold nanoparticles for electrooxidation and sensitive determination of nitrite. *Biosens. Bioelectron.* **2014**, *51*, 379–385. [[CrossRef](#)]
45. Huang, X.; Li, Y.; Chen, Y.; Wang, L. Electrochemical determination of nitrite and iodate by use of gold nanoparticles/poly(3-methylthiophene) composites coated glassy carbon electrode. *Sens. Actuators B* **2008**, *134*, 780–786. [[CrossRef](#)]
46. Pham, X.-H.; Li, C.A.; Han, K.N.; Huynh-Nguyen, B.-C.; Le, T.-H.; Ko, E.; Kim, J.H.; Seong, G.H. Electrochemical detection of nitrite using urchin-like palladium nanostructures on carbon nanotube thin film electrodes. *Sens. Actuators B* **2014**, *193*, 815–822. [[CrossRef](#)]

47. Fu, L.; Yu, S.; Thompson, L.; Yu, A. Development of a novel nitrite electrochemical sensor by stepwise in situ formation of palladium and reduced graphene oxide nanocomposites. *RSC Adv.* **2015**, *5*, 40111–40116. [[CrossRef](#)]
48. Gowda, J.I.; Nandibewoor, S.T. Electrochemical behavior of paclitaxel and its determination at glassy carbon electrode. *Asian J. Pharm. Sci.* **2014**, *9*, 42–49. [[CrossRef](#)]
49. Heli, H.; Eskandari, I.; Sattarahmady, N.; Moosavi-Movahedi, A.A. Cobalt nanoflowers: Synthesis, characterization and derivatization to cobalt hexacyanoferrate—Electrocatalytic oxidation and determination of sulfite and nitrite. *Electrochim. Acta* **2012**, *77*, 294–301. [[CrossRef](#)]
50. Zhang, S.; Li, B.Q.; Zheng, J.B. An electrochemical sensor for the sensitive determination of nitrites based on Pt-PANI-graphenenanocomposites. *Anal. Methods* **2015**, *7*, 8366–8372. [[CrossRef](#)]
51. Balasubramanian, P.; Velmurugan, M.; Chen, S.-M.; Chen, T.-W.; Ye, Y.-T. A single-step electrochemical preparation of cadmium sulfide anchored ERGO/ β -CD modified screen-printed carbon electrode for sensitive and selective detection of nitrite. *J. Electrochem. Soc.* **2019**, *166*, B690–B696. [[CrossRef](#)]
52. Caetano, L.P.; Lima, A.P.; Tormin, T.F.; Richter, E.M.; Espindola, F.S.; Botelho, F.V.; Munoz, R.A.A. Carbon-nanotube modified screen-printed electrode for the simultaneous determination of nitrite and uric acid in biological fluids using batch-injection amperometric detection. *Electroanalysis* **2018**, *30*, 1862–1871. [[CrossRef](#)]
53. Koyun, O.; Sahin, Y. Voltammetric determination of nitrite with gold nanoparticles/poly(methylene blue)-modified pencil graphite electrode: Application in food and water samples. *Ionics* **2018**, *24*, 3187–3197. [[CrossRef](#)]
54. Monteiro, T.; Rodrigues, P.R.; Gonçalves, A.L.; Moura, J.J.G.; Jubete, E.; Añorga, L.; Almeida, M.G. Construction of effective disposable biosensors for point of care testing of nitrite. *Talanta* **2015**, *142*, 246–251. [[CrossRef](#)]
55. State Standard 29299-92. Meat and meat products. In *Determination of Nitrite Content*; Izdatelstvo Standartov: Moscow, Russia, 2003.
56. State Standard 33045-2014. Water. In *Methods for Determination of Nitrogen-Containing Matters*; Izdatelstvo Standartinform: Moscow, Russia, 2019.



© 2020 by the authors. Licensee MDPI, Basel, Switzerland. This article is an open access article distributed under the terms and conditions of the Creative Commons Attribution (CC BY) license (<http://creativecommons.org/licenses/by/4.0/>).